Omnidirectional Bending and Pressure Sensor Based on Stretchable CNT-PU Sponge

Haotian Chen, Zongming Su, Yu Song, Xiaoliang Cheng, Xuexian Chen, Bo Meng, Zijian Song, Dongmin Chen,* and Haixia Zhang*

Bending and pressure sensors are very essential for evaluating external stimuli in human motions; however, most of them are separate devices. Here, two orthogonal carbon nanotube–polyurethane sponge strips (CPSSs) are used, each of which has different resistances when bent or pressed, to fabricate a multi-functional stretchable sensor capable of detecting omnidirectional bending and pressure independently. Due to the shape of the strip, the resistance of CPSS changes differently when bent along different directions. Based on this feature, two perpendicular CPSSs can reflect information of both bending distance and bending direction. After basic measurement data are obtained, a function set can be formulated to calculate bending distance and bending direction simultaneously. The errors of bending distance and bending angle can be controlled to less than 4%. With the help of the triboelectric effect, which only happens when the device is pressed, the sensor can differentiate bending and pressure effectively, ensuring the device works in complex situations.

1. Introduction

Nowadays, with rapid developments of electronic technologies and computer science, robots are expected to be widely used in various fields such as industry,[1–3] rehabilitation assistance,[4–6] and even household.[7–10] In order to complete dexterous manipulation and interaction tasks, robots need to possess more powerful sensing abilities to behave more like humans.

Tactility, unlike sight and audition, enables an exchange of information between robots and the environment and is drawing much attention. To mimic the properties of human skin, electronic skin (e-skin) is required to distinguish a variety of mechanical stimuli such as normal pressure and bending. Meanwhile, it should also ensure mechanical compliance to withstand deformation.

Currently, different mechanisms including transistor sensing,[11–13] capacitive sensing,[14,15] piezoelectric sensing,[16,17] piezoresistive sensing,[18–20] and triboelectric sensing[21,22] are utilized to achieve this goal. Among them, piezoresistive sensors, which are typical sensors that transduce the external stimuli imposed on the sensor to resistance changes, have been widely used owing to their attractive advantages of simple structure and easy signal collection.[20,23] Conventionally, conductive polymer films or elastomeric rubbers filled with conductive materials (particles,[24] nanowires,[8] nanoflakes,[25] etc.) are used as the sensing materials. However, these conductive rubber or thin film sensors are still lacking in sensitivities and are difficult to fabricate in mass production.

Conductive porous sponges or foams are considered as alternative materials for piezoresistive sensors owing to their combinational electrical conductivities, mechanical flexibilities, and porosities.[26] Recently, several conductive sponges with high electrical conductivities and good mechanical properties have been reported. Conductive carbon nanotube sponges constructed via a chemical vapor deposition process[27] and solution dip-coating of conductive nanomaterials on the backbone of commercial sponges[25,28,29] have been developed to generate piezoresistive sensors.

The triboelectric generator[30] is an emerging self-power sensing mechanism based on contact electrification and electrostatic induction. Compared to piezoelectric sensing, the triboelectric generator is not limited to the specific material, which broadens its application fields. The single-friction-surface triboelectric generator (STEG),[31] one of the four basic working modes of triboelectric generator, usually acts as a self-power sensing element due to its simple structure and has been used in many fields such as polymer distinguishing and moving object detection.[32]

For human beings, bending and pressure detection are two of the most common movements in daily life. Development of an effective multi-functional sensor becomes an urgent

H. Chen, X. Chen, Prof. D. Chen
Academy for Advanced Interdisciplinary Studies
Peking University
Beijing 100871, China
E-mail: dongminchen@pku.edu.cn
Z. Su, Y. Song, X. Cheng, Dr. B. Meng,
Dr. Z. Song, Prof. H. Zhang
National Key Lab of Nano/Micro Fabrication Technology
Institute of Microelectronics
Peking University
Beijing 100871, China
E-mail: zhang-alice@pku.edu.cn
Dr. B. Meng
Beijing Micro Energy Technology Co., Ltd.
Beijing 100190, China

FULL PAPER

problem to be solved. However, recently reported bending sensors only focus on detecting bend in a single direction, such as finger bending detection,[33] which seriously hinders their applications in detection of more complex multidimensional bending conditions. Actually, both bending curvature and direction are important parameters for establishing the hominoid electronic sensor, whose significance is often ignored. Moreover, the piezoresistance-based bending sensor usually suffers from the interference from external pressure, because both bending and pressure can make resistance to change, causing confusion for multi-function detection.[34]

In this paper, we develop a facile, low-cost, and stretchable multi-functional sensor using carbon nanotube–polyurethane (CNT-PU) sponge, which can detect omnidirectional bending and pressure independently. The omnidirectional bending detection provides the information of both bending direction and curvature simultaneously. This relies on two CNT-PU sponge strips (CPSSs) intersecting each other, whose electrical resistances depend on bending curvature and direction due to their shape. This curvature and direction-sensitive sensor is very useful in the applications such as detecting multidirectional joint bent and deformation of soft substrate such as human skin. What's more, a new kind of sensing mechanism, triboelectric sensing, is utilized, serving as an assistant signal to pressure signal in order to make the sensor differentiate between pressure and bending.

2. Fabrication and Basic Characters of Multi-Functional Sensor

The multi-functional sensor is composed of two orthogonal functional layers, each consisting of a CPSS and a polydimethylsiloxane (PDMS) substrate. The schematic fabrication process is shown in **Figure 1**a. At first, uniformly dispersed CNT ink is

prepared and then a carefully cut commercial PU sponge strip is immersed into the CNT ink for 5 min. Then, the CPSS is put into the dry oven at 120 °C to make the water in the ink to evaporate fast. After several times of the dip-coating process, the PU sponge is fully coated by CNTs inside and out through this feasible method. CPSS is put on the half-cured PDMS and they are cured together to make CPSS tightly adhered on the PDMS. Half-cured PDMS is the key point for fabricating the functional layer. If the PDMS is fully cured, the CPSS cannot attach on its surface. If the PDMS is in the liquid state, when the CPSS is put into it, the uncured PDMS will quickly permeate into the sponge and the porosity of the sponge is lost, which will decrease the sensitivity. At last, two of such functional layers were assembled intersecting with each other, each functional layer acting as single axis (x or y) bending sensors. Optical photographs of this integrated structure of the resultant double axial sensor are shown in Figure 1b. The fabrication process is very simple and the device can easily tolerate very large bending movement without damage, as shown in Figure 1c.

Figure 1d,e shows scanning electron microscopy (SEM) images of the CPSS surface. The pore scale of the sponge ranges from 0.5 to 1 mm. From Figure 1e, it can be seen that the CNTs are uniformly coated on the backbone of the sponge. More detailed information on material preparation and device fabrication can be found in Figure S1 (Supporting Information) in the Experimental Section.

The concentration of CNT ink and dip times are two main factors to influence the resistance of the device. In this experiment, the concentration of CNT ink is fixed and the resistance is controlled by dip times. **Figure 2**a shows the relationship of dip times and the resistance. For the first time, the resistance is as high as 450 kΩ. As the dip time continues to increase, the resistance decreases dramatically until it gets saturation at the fifth time and the resistance decreases to 2.3 kΩ. After that,
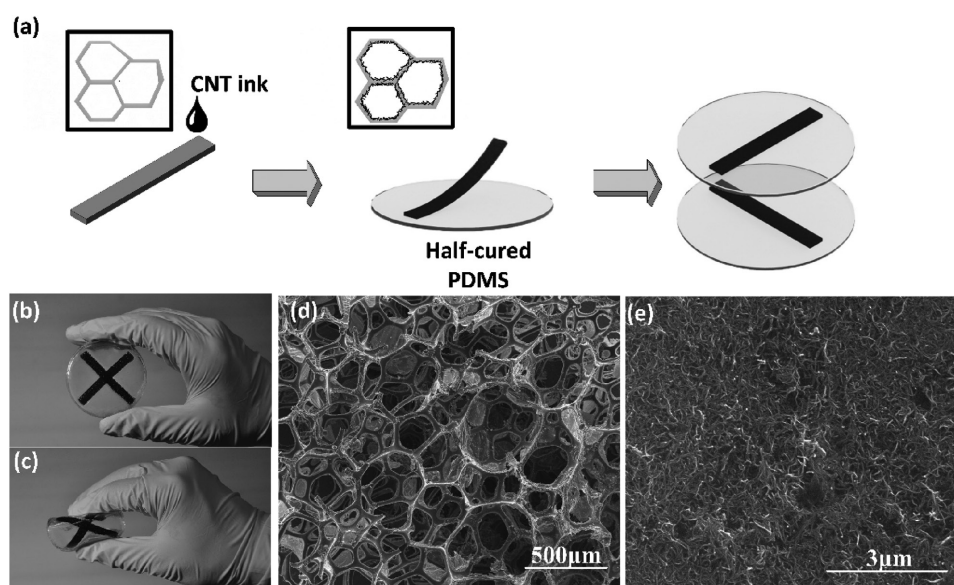

Figure 1. Fabrication and characterization of CPSS-based bending sensor. a) Fabrication process of the sensor, including dip CNT ink on the sponge, putting the CPSS on the half-cured PDMS and assembling two functional layers perpendicularly. b,c) Optical pictures of the sensor: I. normal condition, II. bending condition. d) SEM of the CNT-sponge in large scale. e) SEM of a backbone of CNT-sponge in small scale showing that CNTs fully adhere on the sponge.
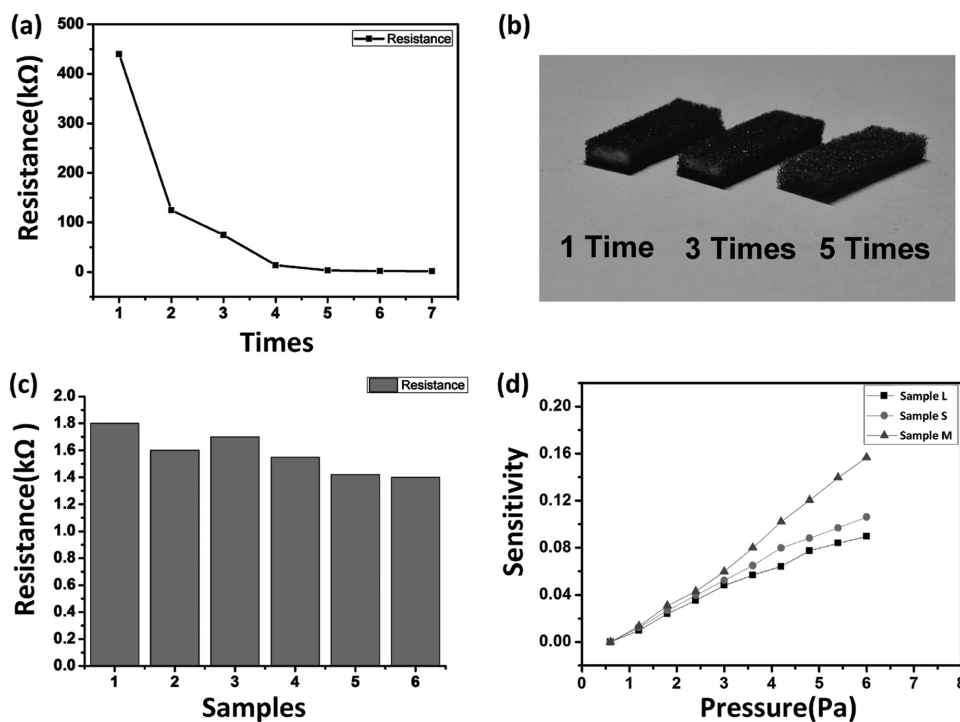
**ADVANCED
SCIENCE NEWS**
www.advancedsciencenews.com

**ADVANCED
FUNCTIONAL
MATERIALS**
www.afm-journal.de

FULL PAPER

Figure 2. Influence factors of CPSS. a) The relationship of resistance and dip times. b) Cross section of three CPSSs with different dip-coating times. c) Resistance histograms of six CPSSs. d) Sensitivities of sensors fabricated by different resistances.

the resistance decreases very slowly, as almost all the backbones of the sponge are covered by CNT. From the cross sections of sponges shown in Figure 2b, at the first time, the CNTs are only adhered on the outer shell of the sponge while the core of the sponge is still clear. The thickness of the CNT shell is about 1 mm. As the dip-coating times increase, the thickness of the CNT shell continues to increase until the fifth time. More SEM pictures can be seen in Figure S1 (Supporting Information) for more details. In order to evaluate the stability of this simple fabrication process, resistances of eight CPSS samples are shown in Figure 2c. The average resistance of these samples is 1.83 kΩ and the most deviation is only 2%.

For different functional layers composed of CPSSs with different resistances, they have different sensitivities under the same pressure. Figure 2c shows the sensitivities of three different resistance sensors, indicating that the middle resistance (33 kΩ) CPSS (Sample M) has the highest sensitivity compared to the large one (85 kΩ) (Sample L) and the small one (1.8 kΩ) (Sample S). This high sensitivity can be explained as follows. As the CPSS is bent or pressed, the central part of the strip is deformed, leading neighboring sponge bones to contact each other so that the contact area of CNTs is increased, resulting in the decrease of resistance. For Sample L, due to the fewer times of dithe p-coating process, CNTs are only attached around the shell of the sponge while the core remain clears as sh,own in Figure 2b. Therefore, the sensitivity of Sample L is not as high as Samples M and S because of fewer contact areas induced by pressure. According to percolation theory,[35] more CNTs enable higher conductance and stability. In this way, when the sponge is deformed, the CNT network in Sample M is easier to change its structure than Sample S, leading to higher sensitivity. The

thickness of the PU sponge will also influence the sensitivity of the sensor. Two types of commercial PU sponge with thicknesses of 0.4 and 0.3 cm are taken to compare their sensitivities. In the pressure test, it can be seen that the thicker sponge has higher sensitivity than the thinner one. This result can be attributed to the change of thickness, which can make more CNT to contact to decrease the resistance. More experiment and simulation results are shown in Figure S2 (Supporting Information).

3. Electrical Properties under Bending

For a single functional layer bending, the resistance of the device is determined by both the direction of bend and curvature. When the device is bent at its most effective direction, the sensitivity is the highest, while when it is bent at the least effective direction, the resistance changes slightly. A bending direction line marked in **Figure 3**a is used to define the direction of the bend, which means the sensor bends along this line under external force. The angle rotated from the most effective direction (along the CPSS itself) to the bending direction line is defined as θ, which we call bending angle in our experiment. Curvature is a parameter to describe bend; however, it is difficult to measure directly. For convenience, the original diameter of the round substrate is L. After bend, the straight line distance between two ends of CPSS is L′. The changed length of ΔL, which we call bending distance in our experiment, is used to replace curvature as shown in Figure 3b.

The basic working principle of a single functional layer is simulated by finite element analysis method (COMSOL software)
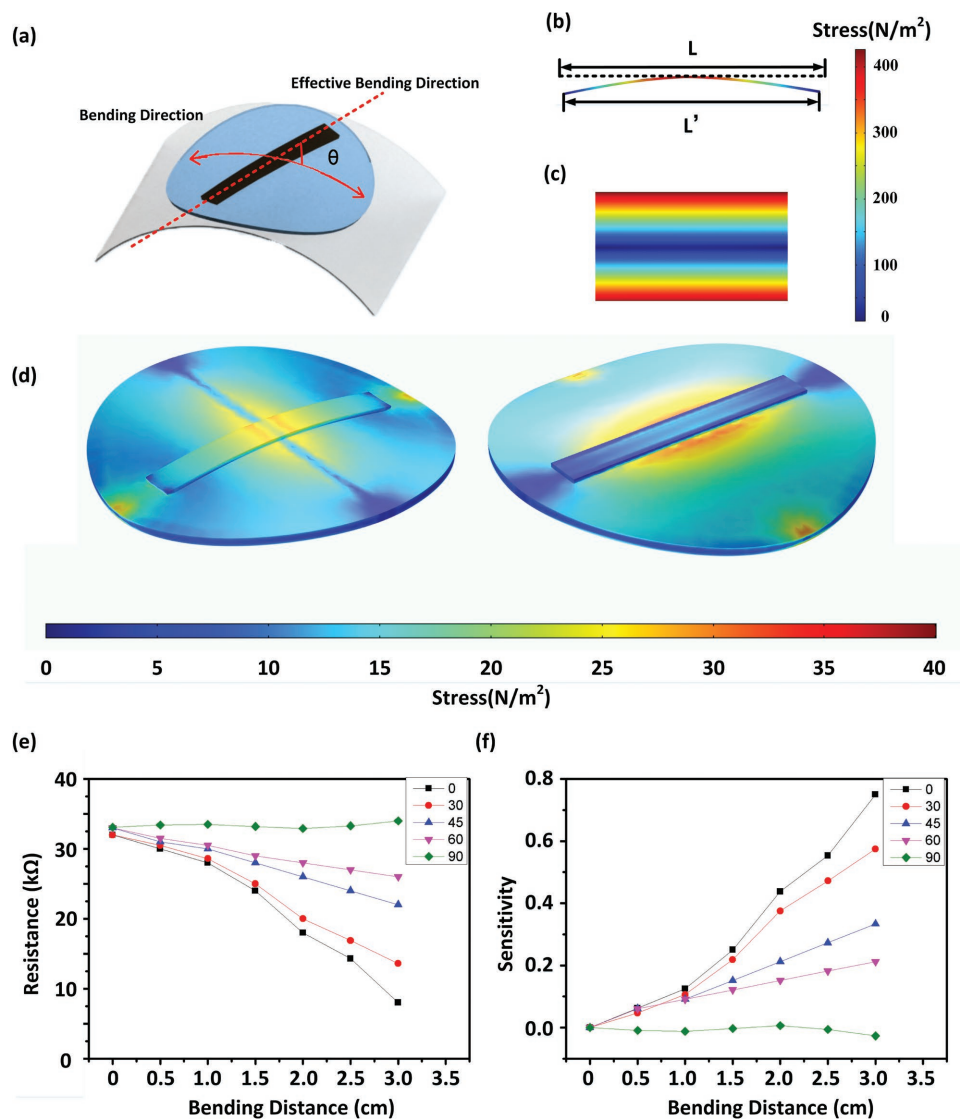
ADVANCED
FUNCTIONAL
MATERIALS
www.afm-journal.de

ADVANCED
SCIENCE NEWS
www.advancedsciencenews.com

FULL PAPER

Figure 3. Working principle of experiment of a single functional layer. a) Definition of bending direction. b) Simulated result of strain of the CPSS in the view of a beam. c) Simulated strain result of the cross section of CPSS. d) Simulated result of the whole functional layer when bent along different direction. e,f) Experimental results of the bending test.

and shown in Figure 3b–d. When CPSS is bent, shown in Figure 3b, the strain is distributed along the whole strip axisymmetric and the largest strain exists at the center of the sponge. At the cross section of the center, the distribution of the absolute value of strain is shown in Figure 3c, where the top surface sustained a stretch while the bottom surface sustained a compression. To study the property of elastic porous material, a honeycomb model is usually utilized, which is described in Figure S3 (Supporting Information) in detail. Poisson's ration of porous is large or nearly zero depending on whether it is stretched or compressed. In our case, strain of top surface makes the thickness of the sponge decrease. From the view of microscale, the decreased thickness means increasing contact areas of CNTs, leading the resistance of the whole sponge to decrease.

Considering the whole functional layer bent at different direction, as shown in Figure 3d, in case I, when the functional layer is bent along the direction of its length, the stress exerted on the sponge is about 28 N. When it comes to case II where the functional layer is bent perpendicular to the direction of the length of CPSS with the same force, the stress decreases to 13 N, which is half of the former situation. Meanwhile, it can be seen from the simulated results in case I, the stress mainly concentrates on the center of the sponge strip, while in case II, the stress is almost uniformly distributed on the whole sponge strip and joint between CPSS and PDMS suffer a lot of stress.

Bending angles of 0°, 30°, 45°, 60°, and 90° and bending distances of 0, 0.5, 1, 1.5, 2, 2.5, and 3 cm are taken as standard bending angles and distances. As shown in Figure 3e,f, when the device bends at a bending angle of 0°, meaning it bends at the most effective direction, the sensitivity of the sensor can reach 6.6 kΩ cm^{-1}. However, when the device bends at 90°,
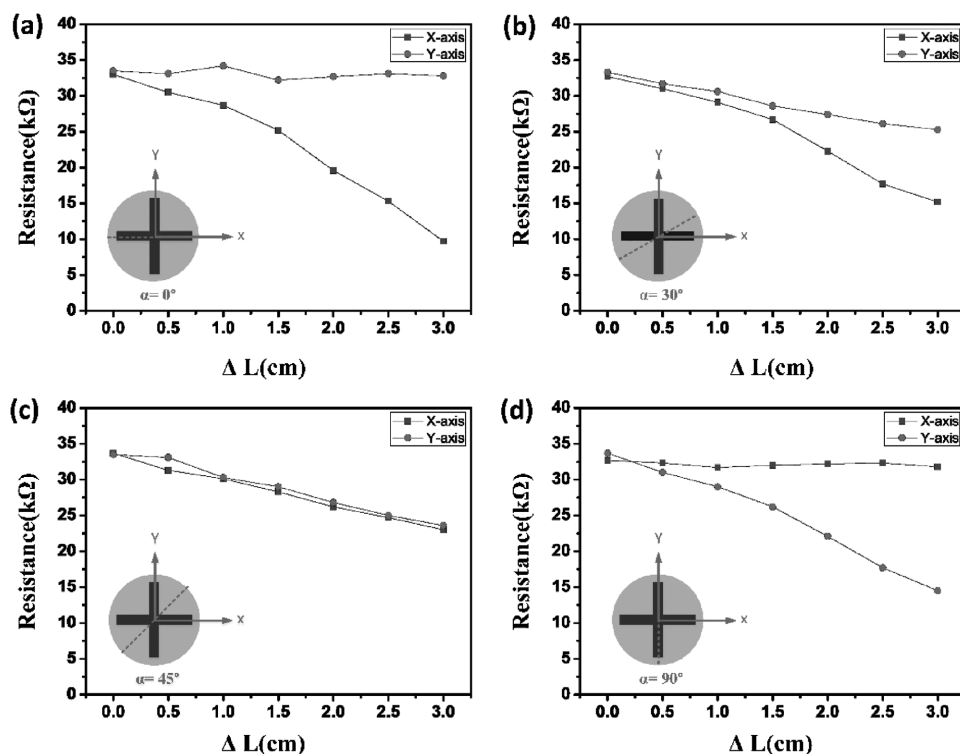
Figure 4. Experimental result of the whole sensor bending at a) 0°, b) 30°, c) 45°, and d) 90°.

the resistance is nearly unchanged, which means it is bent at the least effective direction. At different bending directions, the sensor presents different sensitivities. The relationship of bending distance and resistance is nearly linear no matter what direction the device is bent.

Since a single functional layer gets the direction-determined sensitivity, the value of the resistance cannot reflect useful information, as it may be caused by long bending distance at large bending angle or by short bending distance at small bending angle. Making use of two perpendicular functional layers can solve this problem. Bending direction and bending degree can be calculated at the same time according to both of their resistances.

Figure 4 demonstrates the experiment results of the assembly consisting of two perpendicular functional layers. The effective direction of bottom functional layer is defined as *x*-axis, and correspondingly, the effective direction of top functional layer is defined as the *y*-axis. The bending angle of the whole sensor is defined as the angle rotated from the *x*-axis to the actual bending direction, which is marked using red dotted line shown in Figure 4. Following the same experimental standard of bending distances and angles, the result clearly shows that when the device is bent at a specific direction, two functional layers give rise to different responses. As the bending direction line is along *x*-axis, the top layer has the least sensitivity while the bottom layer has the highest sensitivity. Oppositely, when the sensor is bent along *y*-axis, the resistance of the top layer changes a lot while the resistance of bottom layer is stable. For the specific bending angle of 45°, the slopes of both the functional layers are almost the same.

4. Analysis and Application

In order to precisely calculate the bending direction and bending degree using two orthotropic CPSSs, a function set is required to describe the relationship of how the bending direction and bending distance influence the resistance according to the experiment result. For a traditional single direction bending sensor, the function is usually expressed as

$$\Delta R = k \cdot \Delta L \tag{1}$$

where ΔR is changed resistance, ΔL is changed bending distance, and k is the slope in the relation of ΔR and ΔL. In our experiment, the function is more complicated because there exists another key parameter, bending angle, that needs to be written into the function. We creatively write the new function for a single functional layer as

$$\Delta R = k \cdot \cos(\theta) \cdot \Delta L \tag{2}$$

where direction angle is introduced into the function and served as a parameter influencing the slope, which correspond to our experiment. According to the result from simulation and experiments, when bending along the least effective direction, the resistance of CPSS is almost unchanged. So, the bending can be decomposed orthogonally along the most effective direction and the least effective direction. When the sensor is bent with the bending angle of θ, the bending B can be decomposed as $B \cdot \cos(\theta)$ along the most effective direction and $B \cdot \sin(\theta)$ along the least effective direction. Only the bending along the most

**ADVANCED
FUNCTIONAL
MATERIALS**

www.afm-journal.de

**ADVANCED
SCIENCE NEWS**

www.advancedsciencenews.com

effective direction makes resistance to change, so Equation (2) is written in the form of cosine. The x-axis is defined using the bottom, so the form of cosine is only appropriate for the bottom functional layer. For the top functional layer, the most effective direction is perpendicular to the bottom one, so the component of $B \cdot \sin(\theta)$ is effective for the top functional layer. With the bending angle of 0°, $\cos(\theta)$ equals 1, which is equivalent to the single CPSS. With the bending angle of 90°, it is equal to 0 (as $\cos(90°) = 0$), which is consistent with the experimental results. For the sensor consisting of double functional layers, the function set can be written as

$$
\begin{cases}
\Delta R_{\text{top}} = k \cdot \sin(\theta) \cdot \Delta L \\
\Delta R_{\text{bottom}} = k \cdot \cos(\theta) \cdot \Delta L
\end{cases}
\tag{3}
$$

where the definition of θ is as same as previously mentioned.

After fitting, k is 6.956, r square is 0.9385, and root-mean-square error (RMSE) is 1.95, indicating that the function set can fit the standard data well. **Figure 5**a,b shows the fitting results for the bottom layer and top layer according to the data collected from previous experiments, respectively. In order to better analyze the fitting result, contour plot is used to describe the result, as shown in Figure 5c,d. In this way, once the resistances of both functional layers are obtained, two contours can be drawn in one plane according to the function set, and the two contours will have an intersection. From the coordinates of the intersection point of these two curves, bending distance and bending angle can be calculated. There are two errors here: distance error and direction error. Absolute distance error is the difference of real bending distance and calculated bending distance, and relative distance error is the ratio of the absolute distance error and the length after bending of CPSS. Similarly, absolute direction error is the difference of real bending angle
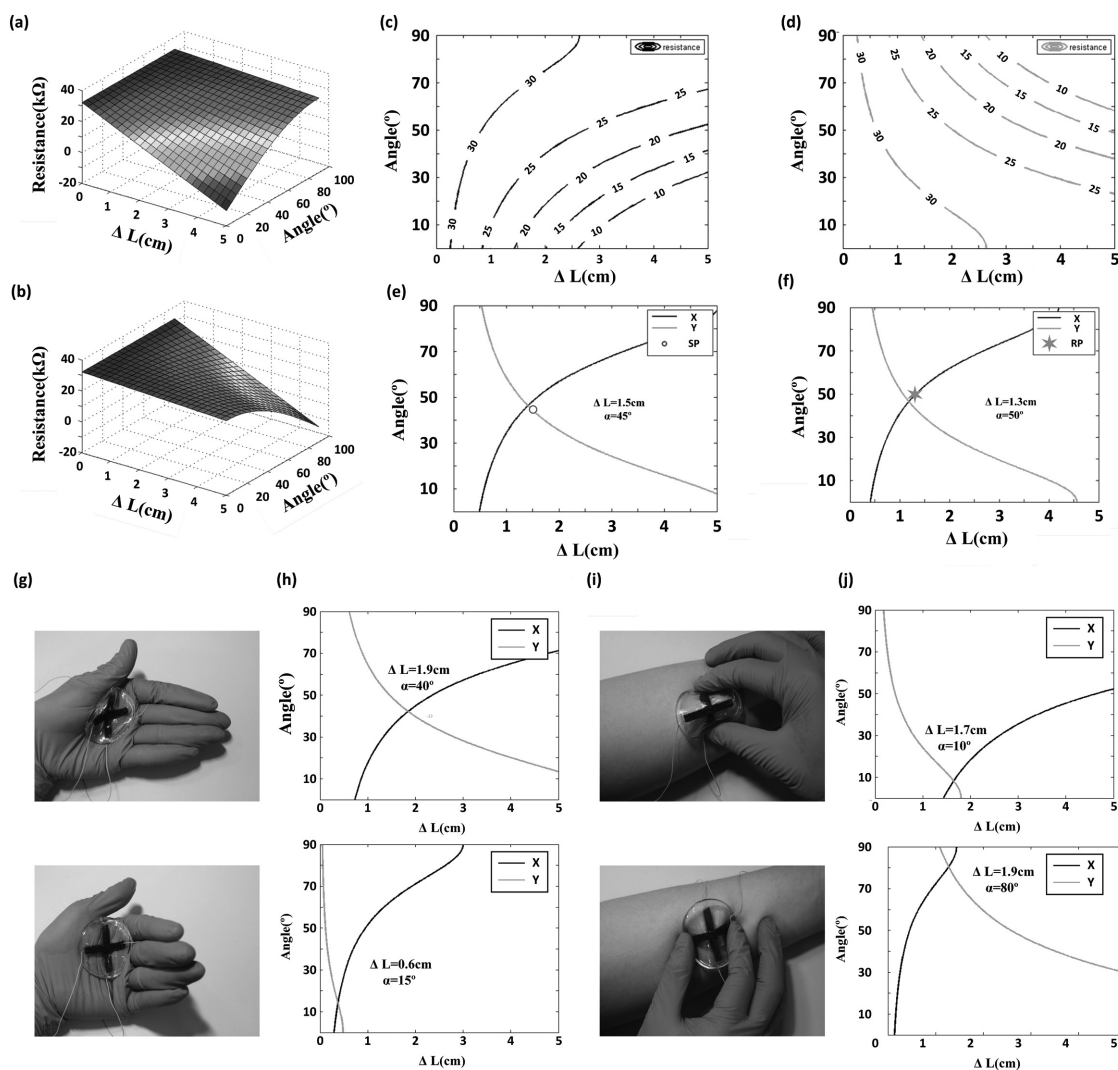

Figure 5. Fitting result of the omnidirectional bending sensor. a,b) 3D fitting result based on experimental data. c,d) Contour result based on experimental data. e) The difference of calculated result and standard test result with bending distance of 1.5 cm and bending direction of 45°. f) The difference of calculated result and real test result with bending distance of 1.3 cm and bending direction of 50°. g,h) Demonstration of sensor located on the palm to detect the movement of the hand. i,j) Demonstration of sensor located on the forearm to detect the deformation of the skin.

**ADVANCED
SCIENCE NEWS**
www.advancedsciencenews.com

**ADVANCED
FUNCTIONAL
MATERIALS**
www.afm-journal.de

FULL PAPER

and calculated bending angle and relative direction error is the ratio of the absolute direction error and angle after bending. In this paper, relative error is used to analyze our calculated results. Standard experiment results are first used to verify the accuracy of the fitting result. In Figure 5e, a bending distance of 1.5 cm and bending direction of 45° is demonstrated in the picture using a circle marked as standard point (SP). Comparing the calculated result and experiment result, the relative distance error is 2.96% and the relative direction error is 3.08%. In order to more explicitly describe the error, total error is defined as the sum of the squares of these two errors, and the total errors of this condition is 4.27%. The error is so small that our fitting function is verified to be useful and effective. After that, random bending distance and bending angle are chosen to test the fitting result. In Figure 5f, the bending distance is 1.3 cm and bending direction is 50°, marked in the picture using a star named random point (RP), while the calculated distance is 1.2 cm and calculated direction is 52°, with a total error of 4.87%. Although the error is larger compared to the standard measurement, the result is acceptable and can definitely tell us the bending distance and bending direction. More of the test results can be seen in Figure S4 (Supporting Information).

This omnidirectional bending sensor is very useful for detecting movement of joints, which usually possess multi-degrees of freedom. As shown in Figure 5g, the device is put on the center of the human palm. There are two bending directions: one is moving the thumb, and the other is moving the other four fingers. Using the omnidirectional bending sensor, it can not only be detected whether the thumb is moving or the other four fingers are moving but also the bending degree of them. When the thumb moves, the resistance of the bottom layer is 26.2 kΩ and resistance of the top layer is 27.7 kΩ. According to the function set, it can be calculated that the change of resistance is induced by thumb (40°) and the bending distance is 1.9 cm. When the other four fingers move, only one resistance changes obviously, indicating that the bending distance is 0.4 cm at 15°, shown in Figure 5h.

Another advantage of this sensor is that it can detect deformation of skin, which is often neglected in daily life. For a smart electronic skin, it is very essential to obtain the information how the skin is pinched up. As demonstrated in Figure 5i, the sensor is attached on the forearm of a human being. When the force is applied by two fingers to make the skin deform, the resistances of two CPSSs change differently. With the help of this multidirectional sensor, it can be clearly identified that bending distance is 1.7 cm and bending angle is 10°, as shown in Figure 5j.

5. Excluding the Interference from External Pressure Using Triboelectric Generator

In most cases, the resistance of CPSS is not only induced by bend but also by pressure, so the bend cannot be measured independently from the mechanical stress. To solve this problem, STEG is applied here to supply a self-power signal.

Figure 6a demonstrates the basic working principle of STEG. It depends on the effects of contact electrification and electrostatic induction. At first, there is no net charge existing on
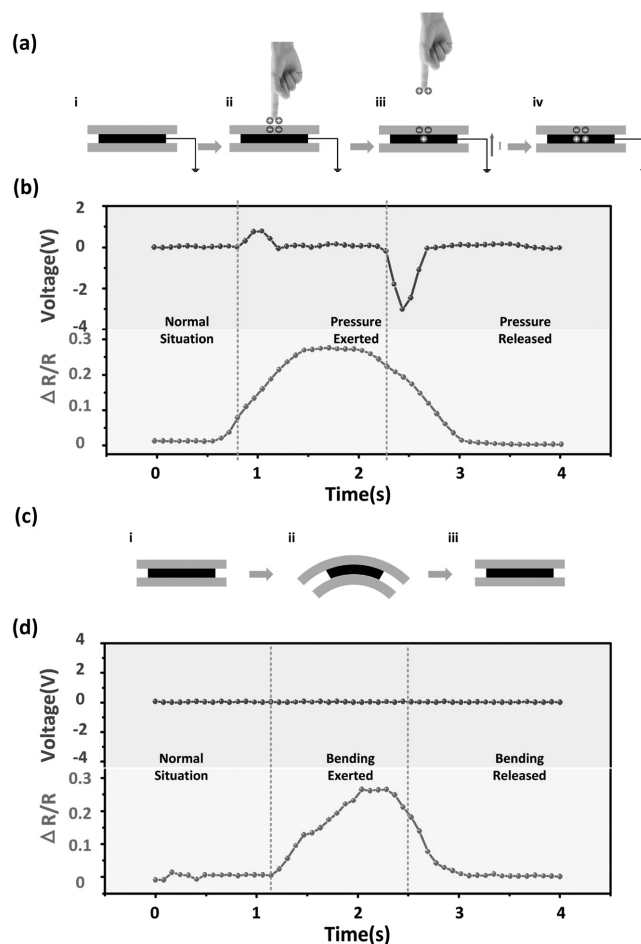

Figure 6. Triboelectric generator helping to rule out the disturbance caused by external stimuli. a) Basic working principle of single-friction-surface triboelectric generator. b) Signals of triboelectric voltage and resistance to distinguish that the changed resistance is caused by exerted pressure. c) Diagram of the bending process. d) Signals of triboelectric voltage and resistance to distinguish that the changed resistance is caused by bending.

the surface of the sensor (i). When an active object (such as a finger) contacts the sensor, the surface of this active object and the friction surface will carry different charges owing to the difference in electron-attracting abilities. In the case of finger tapping, human skin is prone to carry more positive charges while the polymer attracts more negative charges, making both of them electrostatically charged (ii). As the charged active object separates from the friction surface, a potential difference forms between the CPSS and the ground, making electrons transferring via the external load reach an electrostatic equilibrium state (iii, iv).

In this way, the resistance of the sensor responds to both bending and pressure; only pressure produces a triboelectric voltage, which is a useful signal to rule out the interference from pressure. Though the triboelectric output is usually affected by many environmental factors, it only functions as a digital signal to indicate that the changed resistance is caused by bending or pressure. The test diagram is shown in Figure S5 (Supporting Information).

**ADVANCED
FUNCTIONAL
MATERIALS**
www.afm-journal.de

**ADVANCED
SCIENCE NEWS**
www.advancedsciencenews.com

FULL PAPER

Figure 6b presents the result of a real-time monitoring test of this sensor when a finger taps on its surface. In the original state, the triboelectric voltage is 0 V and resistance is stable. When a finger taps on the surface of the sensor, the triboelectric responds very fast and generates a pulse with positive peak value of 0.477 V, and resistance also changes from 35.2 to 27.5 kΩ. The resistance remains unchanged until the finger separates from the surface. At the same time, the STEG generates a pulse with a negative peak value of −3.613 V. The difference in peak values is caused by the speed of separation. As the amount of charges is the same, faster separation shortens the transferring time, causing a higher value of electrical current (demonstrated in Video S1, Supporting Information).

Figure 6c,d presents the process of bending. At first, the triboelectric voltage and resistance are stable. As the sensor is bent, the resistance of CPSS changes fast while the triboelectric voltage is still 0 V, which is a great difference when the sensor is pressurized by a finger. After the sensor recovery from the bending state to normal state, only the change of resistance can be discovered (demonstrated in Video S2, Supporting Information).

Characterization of the STEG voltage is demonstrated in Figure S6 (Supporting Information). The test is conducted under vibration at 5 Hz with equipment described in the Experimental Section. A single cycle of waveform of triboelectric voltage with peak-peak value of 15.07 V is obtained. Using different objects such as hand and nitrile butadiene rubber (NBR) to contact the sensor with the same frequency and amplitudes, the output voltage is different due to the different properties of object themselves. Though the output voltages are influenced by different objects contacting the sensor, the appearance of triboelectric signal can figure out whether an object contacts the sensor.

6. Conclusions

In summary, a stretchable and multi-functional sensor, CPSS, which can detect omnidirectional bending and pressure independently, has been demonstrated in this work. A simple and low-cost method has been promoted in the device fabrication. The porous structure makes it sensitive both to bending and pressure. The electrical property can be easily controlled by concentration of CNT ink and dip time. As a single CPSS has different sensitivities in different bending directions due to its shape, two perpendicular CPSSs are stacked up together to complement the information of bending distances and bending directions at the same time. Based on standard experimental test data, a universal function set has been built up, in which, both of the bending distances and bending directions can be directly obtained with negligible error from two resistances of the double-layer sensor. As bending is a very common action in human motion, this omnidirectional bending sensor is very useful for detecting human motion of multiple degrees of freedom. In addition, with the help of the triboelectric effect, this sensor can effectively avoid the disturbances coming from external pressure through an active sensing method, making it more accurate in complex working conditions.

7. Experimental Section

Fabrication of CNT Ink: CNTs were purchased from Boyu Co., China, with length of 10 μm, and sodium dodecylbenzenesulfonate (SDBS) was purchased from Guoyao Co., China, as a surfactant. The CNT ink was prepared by adding 20 mg CNTs and 20 mg SDBS into 20 mL deionized water and then bath-sonicated for 4 h to disperse evenly.

Fabrication of a Single Functional Layer: PU sponge (purchased from Huayi Co., China, with thickness of 4 mm) was cut into a strip with a length of 3 cm and width of 1 mm. The sponge strip was washed with deionized water and dried in oven at 100 °C. Then the sponge strip was immersed into CNT ink for 1 min and dried at 120 °C for 15 min. As a result, the PU sponge strips were uniformly coated by CNTs, thus generating the basic part of a single functional layer. For the substrate fabrication, 2 g PDMS (Dow Corning, Sylgard 184) was first poured into a plastic petri dish and baked at 70 °C for 20 min. After that, the elastomer mixture was half cured. Then the CPSS was put on the PDMS and baked them together to make the CPSS tightly adhered on the PDMS.

Triboelectric Output Characterization: Experimental measurement was operated using a vibration system, which includes an oscilloscope with wave generation module (Agilent DSO-X 2014A), a modal shaker (JZK-10), and a power amplifier (SINOCERA YE5871A).

Supporting Information

Supporting Information is available from the Wiley Online Library or from the author.

[1] R. Ma, J. Lee, D. Choi, H. Moon, S. Baik, *Nano Lett.* **2014**, *14*, 1944.
[2] J. Kim, M. Lee, H. J. Shim, R. Ghaffari, H. R. Cho, D. Son, Y. H. Jung, M. Soh, C. Choi, S. Jung, K. Chu, D. Jeon, S. T. Lee, J. H. Kim, S. H. Choi, T. Hyeon, D. H. Kim, *Nat. Commun.* **2014**, *5*, 5747.
[3] N. Lu, C. Lu, S. Yang, J. Rogers, *Adv. Funct. Mater.* **2012**, *22*, 4044.
[4] J. Park, Y. Lee, J. Hong, M. Ha, Y.-D. Jung, H. Lim, S. Y. Kim, H. Ko, *ACS Nano* **2014**, *8*, 4689.
[5] X. Huang, Y. Liu, H. Cheng, W. J. Shin, J. A. Fan, Z. Liu, C. J. Lu, G. W. Kong, K. Chen, D. Patnaik, S. H. Lee, S. Hage-Ali, Y. Huang, J. A. Rogers, *Adv. Funct. Mater.* **2014**, *24*, 3846.
[6] D. Kang, P. V. Pikhitsa, Y. W. Choi, C. Lee, S. S. Shin, L. Piao, B. Park, K. Y. Suh, T. I. Kim, M. Choi, *Nature* **2014**, *516*, 222.
[7] J. Lessing, S. A. Morin, C. Keplinger, A. S. Tayi, G. M. Whitesides, *Adv. Funct. Mater.* **2015**, *25*, 1418.
[8] M. Amjadi, A. Pichitpajongkit, S. Lee, S. Ryu, I. Park, *ACS Nano* **2014**, *8*, 5154.
[9] D. J. Cohen, D. Mitra, K. Peterson, M. M. Maharbiz, *Nano Lett.* **2012**, *12*, 1821.
[10] C. Pang, G. Y. Lee, T. I. Kim, S. M. Kim, H. N. Kim, S. H. Ahn, K. Y. Suh, *Nat. Mater.* **2012**, *11*, 795.
[11] J. A. Voorthuyzen, P. Bergveld, A. J. Sprenkels, *IEEE Trans. Electr. Insul.* **1989**, *24*, 267.

**ADVANCED
SCIENCE NEWS**
www.advancedsciencenews.com

**ADVANCED
FUNCTIONAL
MATERIALS**
www.afm-journal.de

FULL PAPER

[12] T. Someya, T. Sekitani, S. Iba, Y. Kato, H. Kawaguchi, T. Sakurai, *Proc. Natl. Acad. Sci. USA* **2004**, *101*, 9966.

[13] T. Someya, Y. Kato, T. Sekitani, S. Iba, Y. Noguchi, Y. Murase, H. Kawaguchi, T. Sakurai, *Proc. Natl. Acad. Sci. USA* **2005**, *102*, 12321.

[14] C. H. Mastrangelo, Z. Xia, W. C. Tang, *J. Microelectromech. Syst.* **1996**, *5*, 98.

[15] C. Metzger, E. Fleisch, J. Meyer, M. Dansachmüller, I. Graz, M. Kaltenbrunner, C. Keplinger, R. Schwödiauer, S. Bauer, *Appl. Phys. Lett.* **2008**, *92*, 013506.

[16] A. V. Shirinov, W. K. Schomburg, *Sens. Actuators, A* **2008**, *142*, 48.

[17] I. Lee, H. J. Sung, *Exp. Fluids* **1999**, *26*, 27.

[18] M. Hussain, Y. H. Choa, K. Niihara, *J. Mater. Sci. Lett.* **2001**, *20*, 525.

[19] T. Yamada, Y. Hayamizu, Y. Yamamoto, Y. Yomogida, A. Izadi-Najafabadi, D. N. Futaba, K. Hata, *Nat. Nanotechnol.* **2011**, *6*, 296.

[20] M. G. King, A. J. Baragwanath, M. C. Rosamond, D. Wood, A. J. Gallant, *Procedia Chem.* **2009**, *1*, 568.

[21] S. Wang, L. Lin, Z. L. Wang, *Nano Energy* **2015**, *11*, 436.

[22] L. Lin, Y. Xie, S. Wang, W. Wu, S. Niu, X. Wen, Z. L. Wang, *ACS Nano* **2013**, *7*, 8266.

[23] S. C. B. Mannsfeld, B. C. K. Tee, R. M. Stoltenberg, C. V. H. H. Chen, S. Barman, B. V. O. Muir, A. N. Sokolov, C. Reese, Z. Bao, *Nat. Mater.* **2010**, *9*, 859.

[24] X. Niu, S. Peng, L. Liu, W. Wen, P. Sheng, *Adv. Mater.* **2007**, *19*, 2682.

[25] Z. Chen, C. Xu, C. Ma, W. Ren, H. M. Cheng, *Adv. Mater.* **2013**, *25*, 1296.

[26] J. W. Han, B. Kim, J. Li, M. Meyyappan, *Appl. Phys. Lett.* **2013**, *102*, 051903.

[27] X. Gui, A. Cao, J. Wei, H. Li, Y. Jia, Z. Li, L. Fan, K. Wang, H. Zhu, D. Wu, *ACS Nano* **2010**, *4*, 2320.

[28] X. Xie, G. Yu, N. Liu, Z. Bao, C. S. Criddle, Y. Cui, *Energy Environ. Sci.* **2012**, *5*, 6862.

[29] Y. Ding, J. Zhu, C. Wang, B. Dai, Y. Li, Y. Qin, F. Xu, Q. Peng, Z. Yang, J. Bai, W. Cao, Y. Yuan, Y. Li, *Carbon* **2016**, *104*, 133.

[30] F.-R. Fan, Z.-Q. Tian, Z. L. Wang, *Nano Energy* **2012**, *1*, 328.

[31] B. Meng, W. Tang, Z.-H. Too, X. Zhang, M. Han, W. Liu, H. Zhang, *Energy Environ. Sci.* **2013**, *6*, 3235.

[32] Y. Su, G. Zhu, W. Yang, J. Yang, J. Chen, Q. Jing, Z. Wu, Y. Jiang, Z. L. Wang, *ACS Nano* **2014**, *8*, 3843.

[33] H. B. Yao, J. Ge, C. F. Wang, X. Wang, W. Hu, Z. J. Zheng, Y. Ni, S. H. Yu, *Adv. Mater.* **2013**, *25*, 6692.

[34] S. Lee, A. Reuveny, J. Reeder, S. Lee, H. Jin, Q. Liu, T. Yokota, T. Sekitani, T. Isoyama, Y. Abe, Z. Suo, T. Someya, *Nat. Nanotechnol.* **2016**, *11*, 472.

[35] J. Li, P. C. Ma, W. S. Chow, C. K. To, B. Z. Tang, J. Kim, *Adv. Funct. Mater.* **2007**, *17*, 3207.